

Radio Burst from a Stellar Coronal Mass Ejection

J. R. Callingham^{1,2*}, C. Tasse^{3,4,5*}, R. Keers^{6,7}, R. D. Kavanagh^{1,2}, H. Vedantham^{1,8}, P. Zarka^{9,5}, S. Bellotti^{10,11}, P. I. Cristofari¹², S. Bloor^{1,8}, D. C. Konijn^{1,8}, M. J. Hardcastle¹³, L. Lamy^{9,5,14}, E. K. Pass^{12,15}, B. J. S. Pope¹⁶, H. Reid¹⁷, H. J. A. Röttgering¹⁰, T. W. Shimwell^{1,10} and P. Zucca¹

¹ASTRON, Netherlands Institute for Radio Astronomy, Oude Hoogeveensedijk 4, Dwingeloo, 7991 PD, The Netherlands.

²Anton Pannekoek Institute for Astronomy, University of Amsterdam, Science Park 904, 1098 XH, Amsterdam, The Netherlands.

³LUX, Observatoire de Paris, Université PSL, CNRS, Meudon, 792190, France.

⁴Centre for Radio Astronomy Techniques and Technologies (RATT), Department of Physics and Electronics, Rhodes University, Makhanda, 6140, South Africa.

⁵Observatoire Radioastronomique de Nançay (ORN), Observatoire de Paris, CNRS, PSL, Université d'Orléans, OSUC, route de Souesmes, Nançay, 18330, France.

⁶Max Planck Institute for Solar System Research, Justus-von-Liebig-Weg 3, 37077, Göttingen, Germany.

⁷Faculty of Electrical Engineering, Information Technology, and Physics, Technische Universität Braunschweig, Hans-Sommer-Strasse 66, 38106, Braunschweig, Germany.

⁸Kapteyn Astronomical Institute, University of Groningen, PO Box 72, 97200 AB, Groningen, The Netherlands.

⁹LIRA, Observatoire de Paris, Université PSL, CNRS, Sorbonne Université, Université de Paris, 5 place Jules Janssen, Meudon, 92195, France.

¹⁰Leiden Observatory, Leiden University, PO Box 9513, 2300 RA, Leiden, The Netherlands.

¹¹Institut de Recherche en Astrophysique et Planétologie, Université de Toulouse, CNRS, IRAP/UMR 5277, 14 avenue Edouard Belin, 31400, Toulouse, France.

¹²Center for Astrophysics, Harvard & Smithsonian, 60 Garden Street, 02138, Cambridge, MA, United States of America.

¹³Centre for Astrophysics Research, University of Hertfordshire, College Lane, AL10 9AB, Hatfield, United Kingdom.

¹⁴Kavli Institute for Astrophysics and Space Research, Massachusetts Institute of Technology, 02139, Cambridge, MA, United States of America.

¹⁵LAM, Aix-Marseille Université, CNRS, CNES, 38 Rue Frédéric Joliot Curie, 13013, Marseille, France.

¹⁶Department of Physics and Astronomy, Macquarie University, NSW 2109, Sydney, Australia.

¹⁷Mullard Space Science Laboratory, University College London, Holmbury, Hill Rd, RH5 6NT, Dorking, United Kingdom.

*Corresponding author(s). E-mail(s): callingham@astron.nl; cyril.tasse@obspm.fr;

Abstract

Coronal mass ejections (CMEs) are massive expulsions of magnetised plasma from a star, and are the largest contributors to space weather in the Solar System [1, 2]. CMEs are theorized to play a key role in planetary atmospheric erosion, especially for planets that are close to their host star [3–5]. However, such a conclusion remains controversial as there has not been an unambiguous detection of a CME from a star outside of our Sun. Previous stellar CME studies have only inferred the presence of a CME through the detection of other types of stellar eruptive events [6–9]. A signature of a fast CME is a Type II radio burst [10, 11], which is emitted from the shock wave produced as the CME travels through the stellar corona into interplanetary space. Here we report an analogue to a Type II burst from the early M dwarf StKM 1-1262. The burst exhibits identical frequency, time, and polarisation properties to fundamental plasma emission from a solar Type II burst. We demonstrate the rate of such events with similar radio luminosity from M dwarfs are $0.84_{-0.69}^{+1.94} \times 10^{-3}$ per day per star. Our detection implies that we are no longer restricted to extrapolating the solar CME kinematics and rates to other stars, allowing us to establish the first observational limits on the impact of CMEs on exoplanets.

Coronal Mass Ejections (CMEs) from the Sun play a fundamental role in shaping the space weather of the Solar System, from driving aurorae to eroding planetary atmospheres [1, 2]. Since the discovery of exoplanets, significant effort has turned to determining the rate and intensities of CMEs around other stars as the persistent impact of CMEs has the potential to strip a planet of its atmosphere [3–5]. We know that younger solar analogues and M dwarfs have much higher flare activity levels than the Sun [12, 13], but it is difficult to know what effect the radically different stellar coronal and magnetospheric conditions will have on the production of CMEs. Understanding CMEs from M dwarfs is particularly pertinent as they host the largest fraction of conventional habitable-zone exoplanets [14]. Since the conventional habitable zones around M dwarfs are substantially closer to the star than in the Solar System [15], the planets around M dwarfs could be subjected to more frequent, higher energy CME impacts than those experienced by Earth [3, 4].

Unfortunately, CMEs are so dim that we have been hitherto restricted to using indirect methods to infer their presence. For example, promising evidence of stellar CMEs includes blueshifts of chromospheric lines [6, 7, 16, 17] and extreme UV/X-ray coronal dimming [8, 9, 18, 19]. However, such Doppler shift and dimming measurements do not inform us if the fast-moving plasma was still retained in the stellar magnetosphere – implying that the plasma may never impact a putative planet. Considering that the magnetic fields of M dwarfs can be over three orders of magnitude stronger than the global solar magnetic field [20], we require a tracer that establishes that plasma has been causally disconnected from the stellar magnetosphere.

One such tracer that reveals that mass has been ejected from a stellar magnetosphere into interplanetary space is a Type II radio burst [21, 22]. A Type II burst is commonly emitted when a CME is super-Alfvénic, implying that a shock has been produced that causally disconnects the plasma from the stellar magnetosphere. The shock excites Langmuir waves as it propagates out of the solar atmosphere, producing coherent radio emission [23]. Type II radio bursts typically last a few minutes, with the emission lanes drifting from high to low frequencies over time, encoding the change in plasma density as the shock propagates. Type II bursts are observed to occur often at both fundamental and harmonic plasma emission frequencies, with the fundamental emission able to reach high brightness temperatures and circular-polarisation fractions [23]. Solar radio observations have demonstrated that there is a strong ($\gtrsim 80\%$) association of Type II bursts with the fastest ($\gtrsim 1800 \text{ km s}^{-1}$) CMEs [10, 11]. While there been rare instances where solar Type II bursts are not associated with CMEs [24], such CMEs have relative slow speeds.

While a Type II burst is unambiguous evidence of plasma escaping from a stellar magnetosphere, there have been no firm detections of Type II bursts from other stars despite significant observational effort [25–29]. The previous non-detections of stellar Type II bursts may be due to sensitivity limitations, the short duration of observations, magnetic confinement of CMEs on radio-bright stars [20], or a high Alfvén speed that prevents shock formation in other

4 *Radio Burst from a Stellar Coronal Mass Ejection*

stellar magnetospheres [30]. Instead, radio observations of M dwarfs have found other types of coherent radio bursts, including hours-long events attributed to the electron-cyclotron maser instability (ECMI) [28, 31–33] that often do not have a direct solar analogue.

Considering that the radio emission of solar Type II bursts is stochastic and occurs predominantly at low frequencies ($\lesssim 300$ MHz), low-frequency wide-field surveys with high sensitivity on timescales of minutes are potentially a powerful tool for discovering a stellar Type II burst. With this aim, we have conducted the LOw-Frequency ARray (LOFAR) Two-metre Sky Survey [LoTSS; 34], covering the Northern sky at sensitivities $\lesssim 2$ mJy per minute. Each ≈ 16 sq. deg. field was targeted for approximately 8 hours, resulting in $\sim 86,000$ stars within 100 pc being observed and searched (Tasse et al., accepted).

During this survey, we detected a stellar swept-frequency radio burst that displays a striking similarity to a solar Type II burst. As shown in Figure 1, the burst lasts for ≈ 2 mins, sweeping from 166 to 120 MHz. This corresponds to a median drift rate of $\approx -0.62 \pm 0.22$ MHz s $^{-1}$, as fit in Figure 2. The burst was detected ≈ 1.2 hours into the LOFAR observation, with no other emission detected in the remaining ≈ 6.8 hours of observation. It has an average flux density of ≈ 110 mJy, but reaches a peak flux density of 440 ± 20 mJy. The burst also appears to display two different lanes of emission, as highlighted in Figure 2, which could be interpreted as band-splitting. Quadratic fits to the two sub-bands are shown in Figure 2, with the emission between the bands potentially analogous to herringbone structures. The burst is highly circularly polarised at an average of $\approx 90\%$, and displays a small amount of linear polarisation for part of its duration ($\approx 10\%$).

As shown in Figure 3, the burst is localised to the active M0V star StKM 1-1262. The star is located at 40.8 pc, is not a known binary, has a 1.241 ± 0.003 d optical photometric rotation signal [35], an effective temperature of 3916 ± 7 K, and a quiescent soft (0.2–2.0 keV) X-ray luminosity of $3.2 \pm 0.1 \times 10^{29}$ ergs s $^{-1}$ (determined from a *XMM-Newton* observation; see Methods). From Zeeman-Doppler imaging, the global magnetic field of StKM 1-1262 has a poloidal-dipolar, non-axisymmetric topology with an average magnetic field strength of ≈ 300 G, and a $v \sin i$ of 25.9 ± 0.2 km s $^{-1}$ (Bellotti et al., accepted). Assuming a stellar radius for an M0V star of $0.63 \pm 0.01 R_{\odot}$ [36], the combination of $v \sin i$ and the measured photometric period implies we are viewing the star equator-on.

With these known characteristics of StKM 1-1262, we can test if the detected burst fits within the solar paradigm of Type II bursts. For example, the velocity of the plasma ejected can be estimated given the drift rate of the burst, coronal scale height of the star, and frequency of emission. As the burst propagates through the stellar corona, the frequency ν of radio emission is expected to vary in time t as [25]

$$\frac{d\nu}{dt} = \frac{\partial \nu}{\partial n_e} \frac{\partial n_e}{\partial h} \frac{\partial h}{\partial s} \frac{\partial s}{\partial t}, \quad (1)$$

where n_e is the electron density, h is radial height above the star, and s is the distance traveled by the shock. For a barometric atmosphere, negligible acceleration, and a shock traveling parallel to our line-of-sight, Equation 1 can be reduced to $\frac{dv}{dt} = -\nu v_s / 2H$, where v_s is the speed of the shock and H the density scale height. The density scale height of StKM 1-1262 can be estimated from its X-ray luminosity (see Methods). For the detected burst, we derive a shock velocity at 144 MHz of $2400 \pm 600 \text{ km s}^{-1}$.

To place this shock velocity into the solar context, $\gtrsim 95\%$ solar CMEs with velocities $\geq 2400 \text{ km s}^{-1}$ are accompanied by a Type II burst [11, 37, 38]. Such a tight correlation is likely because plasma with a velocity exceeding 2400 km s^{-1} is almost always super-Alfvénic, regardless of the local density and magnetic field inhomogeneities in the solar corona [11, 37]. Furthermore, only $\approx 0.05\%$ of CMEs occur with velocities as high as $\geq 2400 \text{ km s}^{-1}$ on the Sun [39], and the average CME rate over the solar cycle is ~ 1.2 per day [39]. If we assume that our sensitivity horizon to Type II bursts is the distance to StKM 1-1262, we have surveyed 5,034 main sequence stars (3,555 stars of spectral type $\sim \text{M0}$ to M6) for 8 hours each in our LOFAR survey (Tasse et al., accepted). Therefore, we could expect ~ 1 burst like that shown in Figure 1, with the same radio luminosity as that observed for Type II bursts on the Sun [38]. This also implies that the rate of such events with similar radio luminosity from M0 to M6 stars are $0.84^{+1.94}_{-0.69} \times 10^{-3}$ per day per star ($1\text{-}\sigma$ uncertainty). Therefore, while the drift rate of the burst and derived velocity are fast, solar Type II bursts have been observed with similar properties [11, 37]. Finally, while we note there are exceptional solar Type II bursts that do not necessarily accompany a CME, in almost all cases this still requires the expulsion of plasma from the magnetosphere of the Sun [40].

While the velocity and morphology of the burst fits within a solar paradigm for Type II bursts, it has other non-standard features. These non-standard features can be explained within the solar Type II emission framework. For example, solar Type II radio bursts are characterised by their emission at both fundamental and harmonic frequencies. Since the circular polarisation fraction of our burst exceeds 60%, it implies that we are detecting emission at the fundamental frequency as only the ordinary mode of the plasma can escape [23]. We do not observe the harmonic emission at later times (top panel, Figure 1). Solar observations demonstrate that it is possible for the harmonic emission never to extend down to as low frequency as the fundamental emission, due to differences in propagation effects, locations of the emission sites, and the group velocities of the electromagnetic waves in the solar corona [38].

Additionally, linear polarisation is canonically expected to be negligible in solar radio bursts due to the high amount of Faraday rotation experienced by the emission as it traverses the corona [41]. However, recent work has challenged such assumptions, with linear polarisation fractions of $\approx 25\%$ detected from solar Type II bursts [42]. The high circular polarisation fraction of the burst is also large for a standard solar Type II burst, but fundamental plasma emission is expected to be generated close to 100% circularly polarised [23].

Fundamental emission from solar Type II bursts are often observed with a low polarisation fractions due to scattering and depolarisation of the emission as it crosses overlying plasma layers in the corona [43]. Therefore, we interpret the preserved high degree of polarisation of our burst as indicative of a relatively clean (i.e. low plasma density and stable magnetic field structure) sight-line to the plasma emission site. Such low-density, stable magnetospheric structures have previously been proposed to exist in M dwarfs due to their strong magnetic fields [28, 29, 32].

Finally, the distance and flux density of the detected burst implies a high brightness temperature for the emission. To derive a physical emitting region, we assume the radio emission occurs at ~ 3 times the stellar radius, calculated by applying a fourfold Newkirk density model for the corona of StKM 1-1262 with a base density of $\sim 0.6 \times 10^{10} \text{ cm}^{-3}$ [38, 44, 45]. Assuming the angular spread of the emission region $\Delta\psi$ is identical to that observed on the Sun [46], namely $\Delta\psi = 13^\circ (r/R_*)^{0.22}$, we find the emitting region is approximately 55% of the photospheric surface of StKM 1-1262. Such an emitting region would produce a brightness temperature of $\approx 1.5 \times 10^{15} \text{ K}$.

Fundamental emission can reach such brightness temperatures, provided the injected hot plasma is ~ 40 times hotter than the ambient coronal temperature of StKM 1-1262 (see Methods). Such temperatures have been measured for flaring M dwarfs [47]. While the ECMI mechanism can recover some of the characteristics of the burst, such as the high circularly polarised fraction and brightness temperature, it struggles to generate the observed frequency sweep unless contrived magnetic geometry and viewing angles are assumed (see Methods). Furthermore, ECMI expects StKM 1-1262 to emit periodically, modulated by the rotation of the star. Follow-up LOFAR observations that have covered the full rotation period of StKM 1-1262 have failed to detect the star again. Finally, the burst would be the most luminous Type II burst detected on the Sun by approximately four-orders of magnitudes. However, the rate we determine in the LoTSS survey at which such luminous bursts occur is broadly consistent with the solar Type II burst rate [48].

Assuming the burst is a stellar Type II burst, we can use its emission characteristics to measure the properties of the ejected plasma from StKM 1-1262. The frequency of the emission of the burst is determined by the electron density $n_e [\text{cm}^{-3}]$ found in the background plasma, namely $\nu = 9 \times 10^{-3} \sqrt{n_e} \text{ MHz}$. The frequency of the emission implies that the density of the plasma ejected is greater than $\sim 3 \times 10^8 \text{ cm}^{-3}$. Assuming the corona of StKM 1-1262 is in hydrostatic equilibrium, the plasma was deposited at ~ 3 times the stellar radius R_* (assuming a base density of $\sim 0.6 \times 10^{10} \text{ cm}^{-3}$, which is common for active M dwarfs [38, 45]). At such a distance, the deposited electron density is an order of magnitude larger than what is commonly simulated for CME impacts on exoplanets [4, 5]. Furthermore, since such radio emission only occurs because the shock is super-Alfvénic, that allows us to put an upper-limit of 19 G for magnetic field of the corona at a distance of $\sim 3 R_*$.

While the magnetic field of the star will determine how such plasma will evolve, if we assume a Parker model and CME mass scaling (total mass $\gtrsim 10^{15}$ g [49]), such a CME will produce a ram pressure of $\gtrsim 0.1 \text{ dyn cm}^{-2}$ at 0.2 AU from StKM 1-1262, the inner boundary of the conventional habitable zone for a M0V star [15]. Such pressure would be capable of compressing planetary magnetospheres to their surface for even a strong terrestrial magnetic field strength of $\sim 3 \text{ G}$ [4].

We have demonstrated that we have detected a radio burst from an M dwarf that has the characteristics of a stellar Type II burst, allowing us to: 1) unambiguously conclude that there has been hot plasma released from StKM 1-1262 into its interplanetary medium; and, 2) calculate the density of the plasma that was released, implying a devastating impact for a putative exoplanet in the conventional habitable zone of StKM 1-1262. Our work means that our empirical benchmarks for the rate and intensities of stellar CMEs are no longer solely determined by the Sun scaled to vastly different stellar magnetic field topologies, ages, strengths, and coronal densities. Our work also supports the rarity of detectable stellar CMEs from M dwarfs, as also suggested by other studies [26]. The detection of such a burst demonstrates we are opening the field of stellar CME studies with LOFAR and the upcoming Square Kilometre Array.

References

- [1] Kouloumvakos, A. *et al.* Properties of solar energetic particle events inferred from their associated radio emission. *Astron. & Astrophys.* **580**, A80 (2015). <https://doi.org/10.1051/0004-6361/201424397> .
- [2] Badruddin, A. & Falak, Z. Study of the geoeffectiveness of coronal mass ejections, corotating interaction regions and their associated structures observed during Solar Cycle 23. *Ap&SS* **361**, 253 (2016). <https://doi.org/10.1007/s10509-016-2839-4> .
- [3] Khodachenko, M. L. *et al.* Coronal Mass Ejection (CME) Activity of Low Mass M Stars as An Important Factor for The Habitability of Terrestrial Exoplanets. I. CME Impact on Expected Magnetospheres of Earth-Like Exoplanets in Close-In Habitable Zones. *Astrobiology* **7** (1), 167–184 (2007). <https://doi.org/10.1089/ast.2006.0127> .
- [4] Kay, C., Opher, M. & Kornbleuth, M. Probability of CME Impact on Exoplanets Orbiting M Dwarfs and Solar-like Stars. *Astrophys. J.* **826** (2), 195 (2016). <https://doi.org/10.3847/0004-637X/826/2/195>, <https://arxiv.org/abs/1605.02683> [astro-ph.SR].
- [5] Varela, J. *et al.* MHD Study of Extreme Space Weather Conditions for Exoplanets With Earth-Like Magnetospheres: On Habitability Conditions and Radio-Emission. *Space Weather* **20** (11), e2022SW003164

- (2022). <https://doi.org/10.1029/2022SW003164>, <https://arxiv.org/abs/2304.08771> [astro-ph.EP].
- [6] Houdebine, E. R., Foing, B. H. & Rodono, M. Dynamics of flares on late-type dMe stars. I. Flare mass ejections and stellar evolution. *Astron. & Astrophys.* **238**, 249 (1990) .
- [7] Vida, K. *et al.* Investigating magnetic activity in very stable stellar magnetic fields. Long-term photometric and spectroscopic study of the fully convective M4 dwarf V374 Pegasi. *Astron. & Astrophys.* **590**, A11 (2016). <https://doi.org/10.1051/0004-6361/201527925>, <https://arxiv.org/abs/1603.00867> [astro-ph.SR].
- [8] Favata, F. & Schmitt, J. H. M. M. Spectroscopic analysis of a super-hot giant flare observed on Algol by BeppoSAX on 30 August 1997. *Astron. & Astrophys.* **350**, 900–916 (1999). <https://doi.org/10.48550/arXiv.astro-ph/9909041>, <https://arxiv.org/abs/astro-ph/9909041> [astro-ph].
- [9] Loyd, R. O. P. *et al.* Constraining the Physical Properties of Stellar Coronal Mass Ejections with Coronal Dimming: Application to Far-ultraviolet Data of Epsilon Eridani. *Astrophys. J.* **936** (2), 170 (2022). <https://doi.org/10.3847/1538-4357/ac80c1>, <https://arxiv.org/abs/2207.05115> [astro-ph.SR].
- [10] Gopalswamy, N. Properties of Interplanetary Coronal Mass Ejections. *Space Science Reviews* **124** (1-4), 145–168 (2006). <https://doi.org/10.1007/s11214-006-9102-1> .
- [11] Gopalswamy, N. *et al.* Coronal mass ejections, type II radio bursts, and solar energetic particle events in the SOHO era. *Annales Geophysicae* **26** (10), 3033–3047 (2008). <https://doi.org/10.5194/angeo-26-3033-2008> .
- [12] Feinstein, A. D. *et al.* Flare Statistics for Young Stars from a Convolutional Neural Network Analysis of TESS Data. *Astron. J.* **160** (5), 219 (2020). <https://doi.org/10.3847/1538-3881/abac0a> .
- [13] Günther, M. N. *et al.* Stellar Flares from the First TESS Data Release: Exploring a New Sample of M Dwarfs. *Astron. J.* **159** (2), 60 (2020). <https://doi.org/10.3847/1538-3881/ab5d3a>, <https://arxiv.org/abs/1901.00443> [astro-ph.EP].
- [14] Dressing, C. D. & Charbonneau, D. The Occurrence of Potentially Habitable Planets Orbiting M Dwarfs Estimated from the Full Kepler Dataset and an Empirical Measurement of the Detection Sensitivity. *Astrophys. J.* **807** (1), 45 (2015). <https://doi.org/10.1088/0004-637X/807/1/45>, <https://arxiv.org/abs/1501.01623> [astro-ph.EP].

- [15] Kasting, J. F., Whitmire, D. P. & Reynolds, R. T. Habitable Zones around Main Sequence Stars. *Icarus* **101** (1), 108–128 (1993). <https://doi.org/10.1006/icar.1993.1010> .
- [16] Namekata, K. *et al.* Probable detection of an eruptive filament from a superflare on a solar-type star. *Nature Astronomy* **6**, 241–248 (2021). <https://doi.org/10.1038/s41550-021-01532-8>, <https://arxiv.org/abs/2112.04808> [astro-ph.SR].
- [17] Namekata, K. *et al.* Discovery of multi-temperature coronal mass ejection signatures from a young solar analogue. *ArXiv e-prints* (2025). <https://doi.org/https://doi.org/10.1038/s41550-025-02691-8>, <https://arxiv.org/abs/2510.22110> [astro-ph.SR].
- [18] Argiroffi, C. *et al.* A stellar flare-coronal mass ejection event revealed by X-ray plasma motions. *Nature Astronomy* **3**, 742–748 (2019). <https://doi.org/10.1038/s41550-019-0781-4>, <https://arxiv.org/abs/1905.11325> [astro-ph.SR].
- [19] Veronig, A. M. *et al.* Indications of stellar coronal mass ejections through coronal dimmings. *Nature Astronomy* **5**, 697–706 (2021). <https://doi.org/10.1038/s41550-021-01345-9>, <https://arxiv.org/abs/2110.12029> [astro-ph.SR].
- [20] Alvarado-Gómez, J. D., Drake, J. J., Cohen, O., Moschou, S. P. & Garraffo, C. Suppression of Coronal Mass Ejections in Active Stars by an Overlying Large-scale Magnetic Field: A Numerical Study. *Astrophys. J.* **862** (2), 93 (2018). <https://doi.org/10.3847/1538-4357/aacb7f> .
- [21] Payne-Scott, R., Yabsley, D. E. & Bolton, J. G. Relative Times of Arrival of Bursts of Solar Noise on Different Radio Frequencies. *Nature* **160** (4060), 256–257 (1947). <https://doi.org/10.1038/160256b0> .
- [22] Wild, J. P. & McCready, L. L. Observations of the Spectrum of High-Intensity Solar Radiation at Metre Wavelengths. I. The Apparatus and Spectral Types of Solar Burst Observed. *Australian Journal of Scientific Research A Physical Sciences* **3**, 387 (1950). <https://doi.org/10.1071/CH9500387> .
- [23] Dulk, G. A. Radio emission from the sun and stars. *Ann. Rev. Astron. & Astrophys.* **23**, 169–224 (1985). <https://doi.org/10.1146/annurev.aa.23.090185.001125> .
- [24] Su, W., Cheng, X., Ding, M. D., Chen, P. F. & Sun, J. Q. A Type II Radio Burst without a Coronal Mass Ejection. *Astrophys. J.* **804** (2), 88 (2015). <https://doi.org/10.1088/0004-637X/804/2/88>, <https://arxiv.org/abs/1503.00861> [astro-ph.SR].

- [25] Crosley, M. K. *et al.* The Search for Signatures of Transient Mass Loss in Active Stars. *Astrophys. J.* **830** (1), 24 (2016). <https://doi.org/10.3847/0004-637X/830/1/24> .
- [26] Crosley, M. K. & Osten, R. A. Low-frequency Radio Transients on the Active M-dwarf EQ Peg and the Search for Coronal Mass Ejections. *Astrophys. J.* **862** (2), 113 (2018). <https://doi.org/10.3847/1538-4357/aacf02> .
- [27] Osten, R. A. & Wolk, S. J. Nandy, D., Valio, A. & Petit, P. (eds) *A Framework for Finding and Interpreting Stellar CMEs*. (eds Nandy, D., Valio, A. & Petit, P.) *Living Around Active Stars*, Vol. 328 of *IAU Symposium*, 243–251 (2017).
- [28] Villadsen, J. & Hallinan, G. Ultra-wideband Detection of 22 Coherent Radio Bursts on M Dwarfs. *Astrophys. J.* **871** (2), 214 (2019). <https://doi.org/10.3847/1538-4357/aaf88e> .
- [29] Zic, A. *et al.* A Flare-type IV Burst Event from Proxima Centauri and Implications for Space Weather. *Astrophys. J.* **905** (1), 23 (2020). <https://doi.org/10.3847/1538-4357/abca90> .
- [30] Alvarado-Gómez, J. D. *et al.* Tuning the Exospace Weather Radio for Stellar Coronal Mass Ejections. *Astrophys. J.* **895** (1), 47 (2020). <https://doi.org/10.3847/1538-4357/ab88a3> .
- [31] Zic, A. *et al.* ASKAP detection of periodic and elliptically polarized radio pulses from UV Ceti. *Mon. Not. R. Astron. Soc.* **488** (1), 559–571 (2019). <https://doi.org/10.1093/mnras/stz1684> .
- [32] Callingham, J. R. *et al.* Low-frequency monitoring of flare star binary CR Draconis: long-term electron-cyclotron maser emission. *Astron. & Astrophys.* **648**, A13 (2021). <https://doi.org/10.1051/0004-6361/202039144>, <https://arxiv.org/abs/2102.04751> [astro-ph.SR].
- [33] Bastian, T. S., Cotton, W. D. & Hallinan, G. Radio Emission from UV Cet: Auroral Emission from a Stellar Magnetosphere. *Astrophys. J.* **935** (2), 99 (2022). <https://doi.org/10.3847/1538-4357/ac7d57>, <https://arxiv.org/abs/2206.14099> [astro-ph.SR].
- [34] Shimwell, T. W. *et al.* The LOFAR Two-metre Sky Survey. V. Second data release. *Astron. & Astrophys.* **659**, A1 (2022). <https://doi.org/10.1051/0004-6361/202142484>, <https://arxiv.org/abs/2202.11733> [astro-ph.GA].
- [35] Colman, I. L. *et al.* Methods for the Detection of Stellar Rotation Periods in Individual TESS Sectors and Results from the Prime Mission. *Astron. J.* **167** (5), 189 (2024). <https://doi.org/10.3847/1538-3881/ad2c86>, <https://arxiv.org/abs/2308.11111> [astro-ph.SR].

- [//arxiv.org/abs/2402.14954](https://arxiv.org/abs/2402.14954) [astro-ph.SR].
- [36] Mann, A. W. *et al.* How to Constrain Your M Dwarf. II. The Mass-Luminosity-Metallicity Relation from 0.075 to 0.70 Solar Masses. *Astrophys. J.* **871** (1), 63 (2019). <https://doi.org/10.3847/1538-4357/aaf3bc>, <https://arxiv.org/abs/1811.06938> [astro-ph.SR].
 - [37] Gopalswamy, N. *et al.* Radio-Quiet Fast and Wide Coronal Mass Ejections. *Astrophys. J.* **674** (1), 560–569 (2008). <https://doi.org/10.1086/524765> .
 - [38] Kumari, A., Morosan, D. E., Kilpua, E. K. J. & Daei, F. Type II radio bursts and their association with coronal mass ejections in solar cycles 23 and 24. *Astron. & Astrophys.* **675**, A102 (2023). <https://doi.org/10.1051/0004-6361/202244015>, <https://arxiv.org/abs/2305.18992> [astro-ph.SR].
 - [39] Gopalswamy, N. *et al.* The SOHO/LASCO CME Catalog. *Earth Moon and Planets* **104** (1-4), 295–313 (2009). <https://doi.org/10.1007/s11038-008-9282-7> .
 - [40] Maguire, C. A., Carley, E. P., Zucca, P., Vilmer, N. & Gallagher, P. T. LOFAR Observations of a Jet-driven Piston Shock in the Low Solar Corona. *Astrophys. J.* **909** (1), 2 (2021). <https://doi.org/10.3847/1538-4357/abda51>, <https://arxiv.org/abs/2101.05569> [astro-ph.SR].
 - [41] Groganard, R. J. M. & McLean, D. J. Non-Existence of Linear Polarization in Type III Solar Bursts at 80 MHz. *Sol. Phys.* **29** (1), 149–161 (1973). <https://doi.org/10.1007/BF00153446> .
 - [42] Dey, S., Kansabanik, D., Oberoi, D. & Mondal, S. First Robust Detection of Linear Polarization from Metric Solar Emissions: Challenging Established Paradigms. *Astrophys. J. Letters* **988** (2), L73 (2025). <https://doi.org/10.3847/2041-8213/ade0e>, <https://arxiv.org/abs/2507.05196> [astro-ph.SR].
 - [43] Stewart, R. T. The polarization of “herring-bone” features in solar radio bursts of spectral type II. *Australian Journal of Physics* **19**, 209 (1966). <https://doi.org/10.1071/PH660209> .
 - [44] Mann, G., Classen, T. & Aurass, H. Characteristics of coronal shock waves and solar type II radio bursts. *Astron. & Astrophys.* **295**, 775 (1995) .
 - [45] Testa, P., Drake, J. J. & Peres, G. The Density of Coronal Plasma in Active Stellar Coronae. *Astrophys. J.* **617** (1), 508–530 (2004). <https://doi.org/10.1086/422355>, <https://arxiv.org/abs/astro-ph/0405019> [astro-ph].

- [46] Crosley, M. K. & Osten, R. A. Constraining Stellar Coronal Mass Ejections through Multi-wavelength Analysis of the Active M Dwarf EQ Peg. *Astrophys. J.* **856** (1), 39 (2018). <https://doi.org/10.3847/1538-4357/aaac2>, <https://arxiv.org/abs/1802.03440> [astro-ph.SR].
- [47] Robrade, J., Poppenhaeger, K. & Schmitt, J. H. M. M. Quiescent and flaring X-ray emission from the nearby M/T dwarf binary SCR 1845-6357. *Astron. & Astrophys.* **513**, A12 (2010). <https://doi.org/10.1051/0004-6361/200913603>, <https://arxiv.org/abs/1002.2389> [astro-ph.SR].
- [48] Giersch, O. D., Kennewell, J. & Lynch, M. Solar Radio Burst Statistics and Implications for Space Weather Effects. *Space Weather* **15** (11), 1511–1522 (2017). <https://doi.org/10.1002/2017SW001658> .
- [49] Gopalswamy, N. & Kundu, M. R. Estimation of the Mass of a Coronal Mass Ejection from Radio Observations. *Astrophys. J. Letters* **390**, L37 (1992). <https://doi.org/10.1086/186366> .

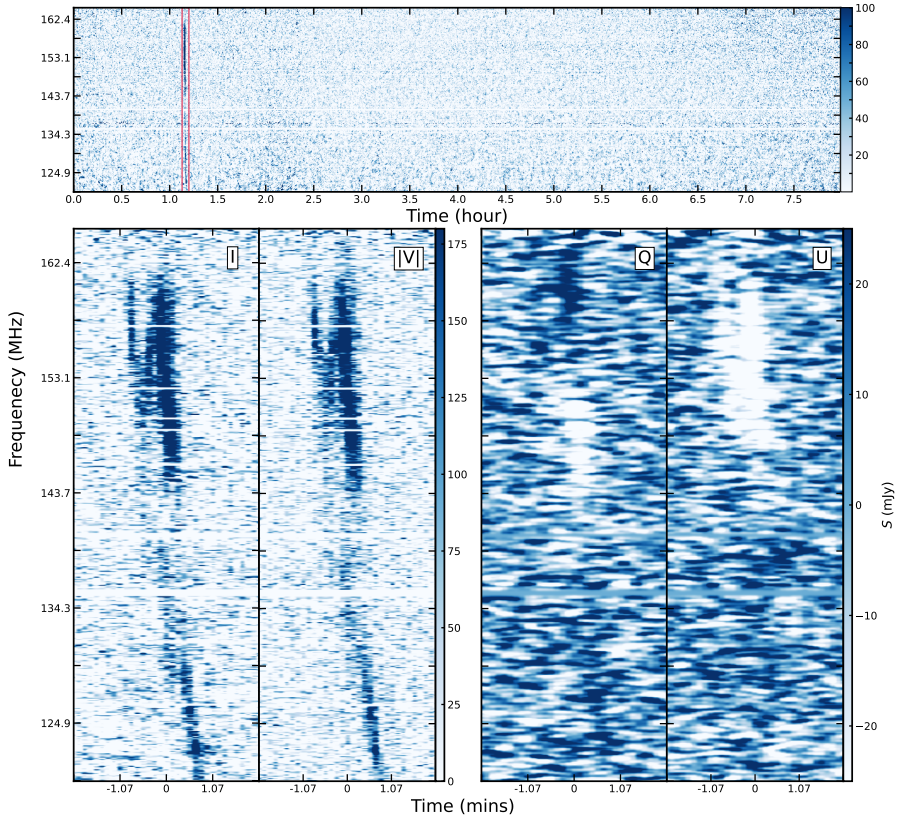


Fig. 1 Dynamic spectra of the burst for different polarisations and durations. The total intensity dynamic spectrum for the entire 8h observation is shown in the top panel, with the burst bracketed by two red lines. The burst is centered in the bottom panels, with Stokes I, absolute V, Q, and U shown left to right, respectively. The dynamic spectra of Stokes Q and U are smoothed with a Gaussian filter with a kernel of 1 pixel to enhance the visibility of the fainter emission. Note that the colour scale of Stokes I and V are different to that of Stokes Q and U, as demonstrated by distinct colour bars.

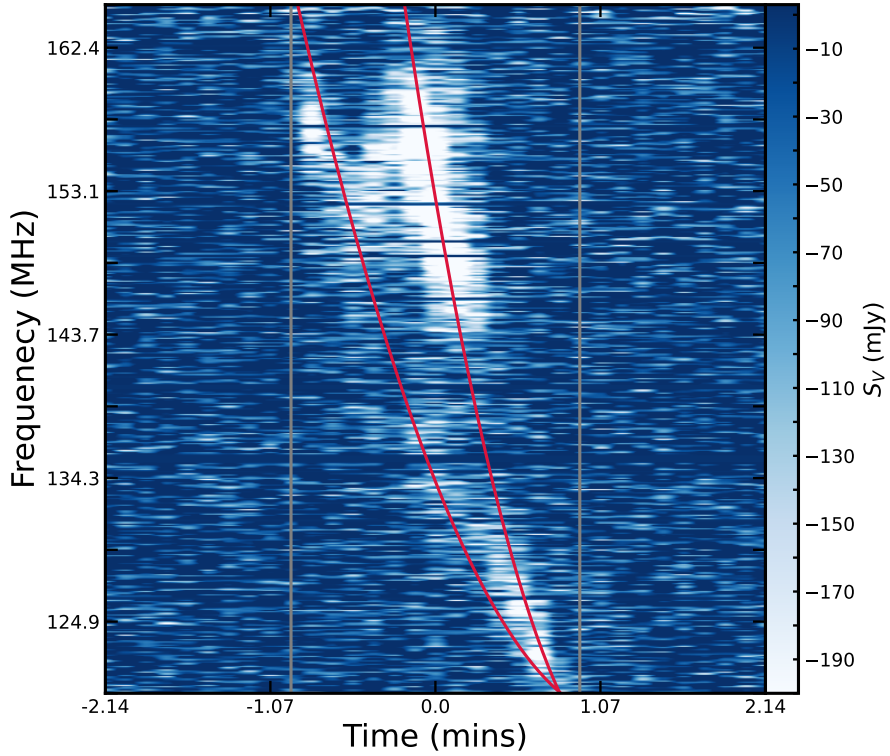


Fig. 2 A ridge-crawler fit to the two different emission lanes evident in the circularly polarised burst. The red lines trace the two fits, and the vertical grey lines demarcate the area over which the fit was searched. The two fits intersect at the lowest frequency channel since that channel contains the largest signal-to-noise at the edge of the band. This is likely a product of the limited bandwidth of our observation.

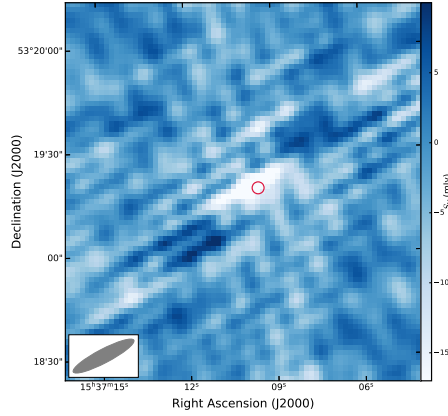


Fig. 3 Circularly polarised dirty map of StKM 1-1262, imaged over the duration of the ≈ 2 minute burst. The red circle identifies the *Gaia* Data Release 3 [50] position of StKM 1-1262 at the time of the LOFAR observation and has a radius of $2''$, corresponding to the astrometric uncertainty of the radio position. The size and shape of the instantaneous synthesised beam is shown in the bottom left corner.

Methods

Radio data acquisition and reduction

The StKM 1-1262 burst discussed here (see Figure 1) was detected as one of the brightest bursts in a radio survey monitoring a predefined sample of $\sim 200,000$ nearby stars using LOFAR [51] data at ~ 150 MHz. Details of the data processing are given in Tasse et al. (accepted), but we give a brief overview here.

The LOFAR Two Meter Sky Survey (LoTSS) [52, 53], initiated in 2016, aims to produce deep, high-resolution images of the northern hemisphere by observing in the $\sim 120 - 165$ MHz frequency range. Upon completion, it will include approximately 3,000 pointings, each involving 8-12 hours of integration, resulting in ~ 340 PB of raw data. To manage this volume, the data is flagged for terrestrial radio frequency interference, averaged, and compressed by a factor of ~ 17 . Producing images with LoTSS is challenging due to the large ~ 5 degree field of view of individual observations, the complexity of antenna primary beams, ionospheric disturbances, and the big data rates. To overcome these obstacles, we developed a method that implements an efficient, wide-field adaptive optics system generalized for polarization [54–56]. The LoTSS pipeline is based in these findings, and operates using the ddf-pipeline¹ framework. By alternating between kMS² and DDFacet³ softwares, ddf-pipeline iteratively solves the direction-dependent calibration and imaging problems, and produces thermal noise-limited, high-fidelity images, in a totally automated way [57].

In order to search for stellar variability within the observation scans, we introduced an additional processing step to the pipeline that consists in coherently averaging the residual visibilities toward selected stellar sources. For a given direction in the sky, path length differences between station pairs are corrected, enabling the formation of dynamic spectra in all four Stokes parameters at the native time and frequency resolution. This step has been implemented in DynSpecMS⁴ software, and accounts for direction-dependent effects, such as ionospheric and primary beam corrections, derived earlier in the pipeline.

The burst of StKM 1-1262 discussed here was detected in an 8h scan, observed on 2016-05-17, and was located ~ 1.4 degrees from the LoTSS pointing center named P236+53, having time and spectral resolution of 8 s and 12.1 kHz. Instrumental leakage between Stokes I and other Stokes parameters was measured to be $\lesssim 1\%$ [58]. This was further confirmed by analysing the dynamic spectra of other non-polarised sources in the field. The average rms noise in the Stokes V dynamic spectrum is ≈ 20 mJy.

To produce Figure 3, we used WSClean [59] with a robust parameter of -0.5 for only the data corresponding to the duration of the burst. Following the

¹<https://github.com/mhardcastle/ddf-pipeline>

²<https://github.com/saopicc/killMS>

³<https://github.com/saopicc/DDFacet>

⁴<https://github.com/cyriltasse/DynSpecMS>

literature in this area [32, 60], we define the sign of the Stokes V emission as left-hand circularly-polarised light minus right-hand circularly-polarised light.

X-ray Data Reduction

On 2006-06-23, *XMM-Newton* serendipitously observed StKM 1-1262 for ≈ 16 ks at $\approx 13'$ away from the pointing centre (ObsID: 0401270201). We processed the observation following established routines [61, 62], utilising the *XMM-Newton* Science Analysis System (SAS) version 20.0.0. Background flares were filtered from the European Photon Imaging Camera data during reduction. Spectral and timing data were extracted from a circular source region with a radius of approximately $16''$, while the background was sampled from a nearby region of double the area on the same CCD. Photon redistribution matrices and ancillary response files were generated for the spectral and timing analysis of the pn, MOS1, and MOS2 cameras using standard calibration files.

The average 0.2 to 10.0 keV count rate for StKM 1-1262 during the observation was ≈ 1.1 counts s^{-1} , and no flares were detected during the observation. The spectrum of StKM 1-1262 was best fit by a single photo-electrically absorbed optically-thin plasma model (XSPEC [63] model `appec`), which provides a 0.2 to 2.4 keV flux of $(1.59 \pm 0.05) \times 10^{-12}$ erg s^{-1} cm^{-2} .

Coronal Scale Height and Plasma Emission

The coronal temperature T_c of StKM 1-1262 was estimated using the relation $T_c = 0.11 F_X^{0.26}$, where F_X represents the X-ray surface flux derived from the 0.2-2.4 keV X-ray luminosity and the photospheric radius of the star [64]. Therefore, the measured soft X-ray flux of $(1.59 \pm 0.05) \times 10^{-12}$ erg s^{-1} cm^{-2} implies a coronal temperature of ~ 7.8 MK.

For estimating the shock velocity, the hydrostatic density structure of the corona of StKM 1-1262 was assumed to have a scale height [65] of $H = 6 \times 10^9 (T_c/10^6 \text{ K}) (R_*/R_\odot)^2 (M_*/M_\odot)^{-1}$ cm, where R_* and M_* are the stellar radius and mass, respectively. The uncertainty on the shock velocity is largely determined by the uncertainty on the drift, and the uncertainty in radius and mass of the star. Consistent with an M0V star, we used a radius of $0.63 \pm 0.02 R_\odot$ and mass of $0.61 \pm 0.01 M_\odot$ for the shock velocity calculation [36].

To calculate the brightness temperature of any potential plasma emission from StKM 1-1262, we varied the temperature of the injected hot plasma to be up to 40 times the measured coronal temperature and applied Equations 15 to 22 of [66]. Such a temperature range is consistent, within an order of magnitude, with the observed temperatures of coronal loops [67] and flares [47] on M dwarfs. It is important to note that the hot component temperature being 40 times the ambient coronal density is chosen as the minimum temperature required to generate the observed brightness temperature, thus should not be the focus of physical interpretation. In particular, the level of

turbulence in our plasma model was assumed to be 10^{-5} , the canonical level at which the turbulence alters the dispersion in the background plasma for fundamental plasma emission [66, 68, 69]. However, a different value for the level of turbulence could vastly change the required temperature of the injected hot component. The point of this exercise is to demonstrate that the properties of the radio emission can be self-consistently explained within a plasma emission model that does not require non-physical values.

Finally, we assumed the Alfvén velocity V_a in the stellar wind of StKM 1-1262 follows $V_a = B/(n_p m_p \mu_0)^{0.5}$, where B , n_p , m_p , and μ_0 are the magnetic field strength, number density of proton, mass of the proton, and magnetic permittivity of free space, respectively. For a Type II burst to occur, the velocity of the shock needs to exceed the Alfvén velocity, implying $v_s > B/(n_p m_p \mu_0)^{0.5}$. Assuming quasi-neutrality ($n_p = n_e$), for $v_s = 2,400 \text{ km s}^{-1}$, the magnetic field strength of the CME at the location of emission must be less than 19 G. Such a magnetic field strength is consistent with a dipole model (or solar model) that has a surface magnetic field strength of 300 G and with the radio emission occurring at three stellar radii.

ECMI emission

An alternative scenario to explain the time-frequency radio sweep observed from StKM 1-1262 is ECMI emission originating in a flaring loop on the stellar surface. ECMI emission is characterised by its beam pattern, which resembles a hollow cone centered on the magnetic field line at the emission site. Due to the anisotropic beam pattern, an observer will generally observe ECMI emission to manifest in short bursts as the emission cone sweeps across the line of sight [70–72]. It also occurs at the local cyclotron frequency, which scales linearly with the local magnetic field strength B [23]

$$\nu = 2.8 \times B \text{ MHz}, \quad (2)$$

where B is in Gauss. Therefore, if ECMI emission occurs along a flaring loop, one can contrive for certain geometric configurations of the viewing angle of the loop from the observer’s perspective to produce a time-frequency sweep akin to that seen from StKM 1-1262 as the star rotates [e.g. 70].

Recently, radio emission from flaring loops on the Sun suggestive of ECMI has been observed [73], albeit without any significant drift in time, which is likely due to the longer rotation period of the Sun compared to StKM 1-1262. To test the viability of the flaring loop scenario for StKM 1-1262, we construct a simple geometric model. We place a circular loop of radius L centered at the stellar surface [e.g. 74]. The co-latitude of the loop center is θ_l , and its longitude at some reference time t_0 is ϕ_l . The loop is misaligned with the meridian by the angle δ_l . The magnetic field strength at the footpoints where the loop meets the surface is B_{fp} . Spatially-resolved observations of ECMI-like emission from flaring loops on the the Sun indicate that the magnetic field strength along the loop drops off roughly linearly with the distance above the

surface [73]. We therefore adopt a linear prescription for the magnetic field strength in the loop, which drops off linearly with the rate m

$$B_l(r) = B_{\text{fp}} - m(r - R_\star), \quad (3)$$

where r is the radial distance between the points on the loop and the centre of the star.

We assume that each point on the flaring loop emits ECMI emission, which is beamed outward in a cone shape. The emission cones are aligned with the magnetic field vector at each point on the loop, each of which being tangent to the loop. The cone opens out from the magnetic field vector by the α , and has a thickness $\Delta\alpha$. We calculate the angle γ between the vector at each emission site and the line of sight, and use it to prescribe the flux density visible to the observer [72]

$$F = F_0 \exp \left[-\frac{1}{2} \left(\frac{\gamma - \alpha}{\Delta\alpha} \right)^2 \right], \quad (4)$$

where F_0 is the maximum flux density visible. In other words, the bulk of the flux density seen when γ is within the range of $\sim \alpha \pm \Delta\alpha/2$. The frequency bins of the dynamic spectrum provide the emission frequency for each point on the loop via Equations 2 and 3, and the time bins provide the longitude of the loop ϕ as a function of time t

$$\phi = \phi_l + \frac{2\pi}{P}(t - t_0), \quad (5)$$

where $P = 1.24$ days is the rotation period.

To explore the likelihood space of the model parameters given the burst shown in Figure 1, we use UltraNest⁵ [75], which utilises the nested sampling Monte Carlo algorithm MLFriends [76, 77]. Uniform priors are assumed for each parameter, which are listed in Extended Data Table 1.

Due to the brightness of the burst, the noise in the dynamic spectrum is not scattered around zero, and instead sits at a value of ~ 20 mJy. To avoid UltraNest attempting to fit this component of the dynamic spectrum, we subtract this value from each pixel prior to running the sampler. The noise of each pixel is ~ 20 mJy. Otherwise, our setup of UltraNest is identical to the approach taken in [72].

Within 50 steps, the sampler converges on the result shown in Figure 1, with a reduced χ^2 of 1.95. While we reproduce the overall drifting structure observed from StKM 1-1262, we cannot recover the finer sub-structure seen in Extended Data Figure 1. The confidence intervals inferred for each model parameter are listed in Extended Data Table 1.

We infer a flaring loop size of $0.3 R_\star$, which is comparable to that obtained on the Sun by [73], which we visually estimate from Figure 4 of [73] to be $\sim 0.2 R_\odot$. Our magnetic field gradient of $9583 \text{ G } R_\star^{-1}$ is also comparable to [73], who obtain a value of $2951 \text{ G } R_\odot^{-1}$ (again estimated visually from

⁵<https://johannesbuchner.github.io/UltraNest/>

their Figure 4). The obtained cone opening angle is also in agreement with observations of ECMI on Jupiter [78].

However, we note the only way to get this model to fit is to have an incredibly thin cone thickness of 0.01° , which is significantly smaller than the $\sim 1^\circ$ inferred from observations of ECMI on Jupiter [79]. While ECMI-like radio bursts have recently been observed on the Sun that could also have such thin cone thickness, such bursts only last for about 10 seconds [see Extended Data Figure 8 of 73].

If the observed burst reported here for StKM 1-1262 and on the Sun by [73] are indeed driven by ECMI, follow-up studies focusing on the theoretical feasibility for producing extremely narrow ECMI will be needed to confirm this scenario. The main issue is that the electron velocity distribution is incredibly small and not predicted by standard theory [e.g. 80].

Another uncertainty about our inferred parameters is the high latitude (or low co-latitude) of the flaring loop. While high-latitude flares on M dwarfs have also been observed [e.g. 81], it remains unclear if this is standard for all M dwarfs since previous studies have been restricted to active, rapidly rotating (<0.5 d) M dwarfs. We also did not re-observe the star in radio despite observing it with LOFAR for subsequent rotations. Radio emission driven by ECMI on M dwarfs have been observed over multiple rotations [32].

References

- [50] Gaia Collaboration *et al.* Gaia Data Release 3. Summary of the content and survey properties. *Astron. & Astrophys.* **674**, A1 (2023). <https://doi.org/10.1051/0004-6361/202243940>, <https://arxiv.org/abs/2208.00211> [astro-ph.GA].
- [51] van Haarlem, M. P. *et al.* LOFAR: The LOw-Frequency ARray. *Astron. & Astrophys.* **556**, A2 (2013). <https://doi.org/10.1051/0004-6361/201220873>, <https://arxiv.org/abs/1305.3550> [astro-ph.IM].
- [52] Shimwell, T. W. *et al.* The LOFAR Two-metre Sky Survey. I. Survey description and preliminary data release. *Astron. & Astrophys.* **598**, A104 (2017). <https://doi.org/10.1051/0004-6361/201629313>, <https://arxiv.org/abs/1611.02700> [astro-ph.IM].
- [53] Shimwell, T. W. *et al.* The LOFAR Two-metre Sky Survey. V. Second data release. *Astron. & Astrophys.* **659**, A1 (2022). <https://doi.org/10.1051/0004-6361/202142484>, <https://arxiv.org/abs/2202.11733> [astro-ph.GA].
- [54] Tasse, C. Applying Wirtinger derivatives to the radio interferometry calibration problem. *ArXiv e-prints* (2014). <https://arxiv.org/abs/1410.8706> [astro-ph.IM].
- [55] Smirnov, O. M. & Tasse, C. Radio interferometric gain calibration as a complex optimization problem. *Mon. Not. R. Astron. Soc.* **449**, 2668–2684 (2015). <https://doi.org/10.1093/mnras/stv418>, <https://arxiv.org/abs/1502.06974> [astro-ph.IM].
- [56] Tasse, C. *et al.* Faceting for direction-dependent spectral deconvolution. *Astron. & Astrophys.* **611**, A87 (2018). <https://doi.org/10.1051/0004-6361/201731474>, <https://arxiv.org/abs/1712.02078> [astro-ph.IM].
- [57] Tasse, C. *et al.* The LOFAR Two-meter Sky Survey: Deep Fields Data Release 1. I. Direction-dependent calibration and imaging. *Astron. & Astrophys.* **648**, A1 (2021). <https://doi.org/10.1051/0004-6361/202038804>, <https://arxiv.org/abs/2011.08328> [astro-ph.IM].
- [58] Callingham, J. R. *et al.* V-LoTSS: The circularly polarised LOFAR Two-metre Sky Survey. *Astron. & Astrophys.* **670**, A124 (2023). <https://doi.org/10.1051/0004-6361/202245567>, <https://arxiv.org/abs/2212.09815> [astro-ph.GA].
- [59] Offringa, A. R. *et al.* WSCLEAN: an implementation of a fast, generic wide-field imager for radio astronomy. *Mon. Not. R. Astron. Soc.* **444**, 606–619 (2014). <https://doi.org/10.1093/mnras/stu1368>, <https://arxiv.org/abs/1407.1943> [astro-ph.IM].

- [60] Callingham, J. R. *et al.* The population of M dwarfs observed at low radio frequencies. *Nature Astronomy* **5**, 1233–1239 (2021). <https://doi.org/10.1038/s41550-021-01483-0>, <https://arxiv.org/abs/2110.03713> [astro-ph.SR].
- [61] Callingham, J. R., Farrell, S. A., Gaensler, B. M., Lewis, G. F. & Middleton, M. J. The X-Ray Transient 2XMMi J003833.3+402133: A Candidate Magnetar at High Galactic Latitude. *Astrophys. J.* **757**, 169 (2012). <https://doi.org/10.1088/0004-637X/757/2/169>, <https://arxiv.org/abs/1108.0697> [astro-ph.HE].
- [62] Callingham, J. R. *et al.* Anisotropic winds in a Wolf-Rayet binary identify a potential gamma-ray burst progenitor. *Nature Astronomy* **3**, 82–87 (2019). <https://doi.org/10.1038/s41550-018-0617-7>, <https://arxiv.org/abs/1811.06985> [astro-ph.SR].
- [63] Arnaud, K. A. Jacoby, G. H. & Barnes, J. (eds) *XSPEC: The First Ten Years*. (eds Jacoby, G. H. & Barnes, J.) *Astronomical Data Analysis Software and Systems V*, Vol. 101 of *Astronomical Society of the Pacific Conference Series*, 17 (1996).
- [64] Johnstone, C. P. & Güdel, M. The coronal temperatures of low-mass main-sequence stars. *Astron. & Astrophys.* **578**, A129 (2015). <https://doi.org/10.1051/0004-6361/201425283>, <https://arxiv.org/abs/1505.00643> [astro-ph.SR].
- [65] Vedantham, H. K. *et al.* Coherent radio emission from a quiescent red dwarf indicative of star-planet interaction. *Nature Astronomy* **4**, 577–583 (2020). <https://doi.org/10.1038/s41550-020-1011-9>, <https://arxiv.org/abs/2002.08727> [astro-ph.EP].
- [66] Stepanov, A. V. *et al.* Microwave plasma emission of a flare on AD Leo. *Astron. & Astrophys.* **374**, 1072–1084 (2001). <https://doi.org/10.1051/0004-6361:20010518>, <https://arxiv.org/abs/astro-ph/0106369> [astro-ph].
- [67] Giampapa, M. S. *et al.* The Coronae of Low-Mass Dwarf Stars. *Astrophys. J.* **463**, 707 (1996). <https://doi.org/10.1086/177284>.
- [68] Benz, A. O. *Plasma astrophysics: Kinetic processes in solar and stellar coronae* Vol. 184 (1993).
- [69] Reid, H. A. S. & Kontar, E. P. Langmuir wave electric fields induced by electron beams in the heliosphere. *Astron. & Astrophys.* **598**, A44 (2017). <https://doi.org/10.1051/0004-6361/201629697>, <https://arxiv.org/abs/1611.07901> [astro-ph.SR].
- [70] Louis, C. K. *et al.* ExPRES: an Exoplanetary and Planetary Radio

- Emissions Simulator. *Astron. & Astrophys.* **627**, A30 (2019). <https://doi.org/10.1051/0004-6361/201935161> .
- [71] Kavanagh, R. D. & Vedantham, H. K. Hunting for exoplanets via magnetic star-planet interactions: Geometrical considerations for radio emission. *Mon. Not. R. Astron. Soc.* (2023). <https://doi.org/10.1093/mnras/stad2035>, <https://arxiv.org/abs/2307.02555> [astro-ph.EP].
- [72] Kavanagh, R. D., Vedantham, H. K., Rose, K. & Bloor, S. Unravelling sub-stellar magnetospheres. *Astron. & Astrophys.* **692**, A66 (2024). <https://doi.org/10.1051/0004-6361/202452094>, <https://arxiv.org/abs/2410.18073> [astro-ph.EP].
- [73] Yu, S. *et al.* Detection of long-lasting aurora-like radio emission above a sunspot. *Nature Astronomy* **8**, 50–59 (2024). <https://doi.org/10.1038/s41550-023-02122-6>, <https://arxiv.org/abs/2310.01240> [astro-ph.SR].
- [74] Titov, V. S. & Démoulin, P. Basic topology of twisted magnetic configurations in solar flares. *Astron. & Astrophys.* **351**, 707–720 (1999) .
- [75] Buchner, J. UltraNest - a robust, general purpose Bayesian inference engine. *The Journal of Open Source Software* **6** (60), 3001 (2021). <https://doi.org/10.21105/joss.03001>, <https://arxiv.org/abs/2101.09604> [stat.CO].
- [76] Buchner, J. A statistical test for Nested Sampling algorithms. *Statistics and Computing* **26** (1-2), 383–392 (2016). <https://doi.org/10.1007/s11222-014-9512-y>, <https://arxiv.org/abs/1407.5459> [stat.CO].
- [77] Buchner, J. Collaborative Nested Sampling: Big Data versus Complex Physical Models. *Publ. Astron. Soc. Pac.* **131** (1004), 108005 (2019). <https://doi.org/10.1088/1538-3873/aae7fc>, <https://arxiv.org/abs/1707.04476> [stat.CO].
- [78] Hess, S., Cecconi, B. & Zarka, P. Modeling of Io-Jupiter decameter arcs, emission beaming and energy source. *Geophys. Res. Lett.* **35** (13), L13107 (2008). <https://doi.org/10.1029/2008GL033656> .
- [79] Kaiser, M. L., Zarka, P., Kurth, W. S., Hospodarsky, G. B. & Gurnett, D. A. Cassini and Wind stereoscopic observations of Jovian nonthermal radio emissions: Measurement of beam widths. *Journal of Geophysical Research (Space Physics)* **105** (A7), 16053–16062 (2000). <https://doi.org/10.1029/1999JA000414> .
- [80] Treumann, R. A. The electron-cyclotron maser for astrophysical application. *Astron. & Astrophys. Rev.* **13**, 229–315 (2006). <https://doi.org/10.1007/s00159-006-0001-0> .

1007/s00159-006-0001-y .

- [81] Ilin, E. *et al.* Giant white-light flares on fully convective stars occur at high latitudes. *Mon. Not. R. Astron. Soc.* **507** (2), 1723–1745 (2021). <https://doi.org/10.1093/mnras/stab2159>, <https://arxiv.org/abs/2108.01917> [astro-ph.SR].

Acknowledgments. This manuscript is dedicated to the memory of Judy Ann Callingham, in recognition of her lifelong support of the first author.

We thank the referees (R. Osten and two anonymous) for their useful comments. JRC acknowledges funding from the European Union via the European Research Council (ERC) grant Epaphus (project number 101166008). RDK and HKV acknowledge funding from the Dutch Research Council (NWO) for the project ‘e-MAPS’ (project number Vi.Vidi.203.093) under the NWO talent scheme VIDI. SB acknowledges funding by the NWO under the project “Exo-space weather and contemporaneous signatures of star-planet interactions” (with project number OCENW.M.22.215 of the research programme “Open Competition Domain Science- M”). PZarka acknowledges funding from the ERC under the European Union’s Horizon 2020 research and innovation programme (grant agreement no. 101020459 - Exoradio). HR acknowledges UKSA grant ST/X002012/1 and STFC grant ST/W001004/1.

The LOFAR data in this manuscript were (partly) processed by the LOFAR Two-Metre Sky Survey (LoTSS) team. This team made use of the LOFAR direction independent calibration pipeline (<https://github.com/lofar-astron/prefactor>), which was deployed by the LOFAR e-infragroup on the Dutch National Grid infrastructure with support of the SURF Co-operative through grants e-infra 170194 e-infra 180169. The LoTSS direction dependent calibration and imaging pipeline (<http://github.com/mhardcastle/ddf-pipeline/>) was run on compute clusters at Leiden Observatory and the University of Hertfordshire, which are supported by a European Research Council Advanced Grant [NEWCLUSTERS-321271] and the UK Science and Technology Funding Council [ST/P000096/1]. The Jülich LOFAR Long Term Archive and the German LOFAR network are both coordinated and operated by the Jülich Supercomputing Centre (JSC), and computing resources on the supercomputer JUWELS at JSC were provided by the Gauss Centre for Supercomputing e.V. (grant CHTB00) through the John von Neumann Institute for Computing (NIC).

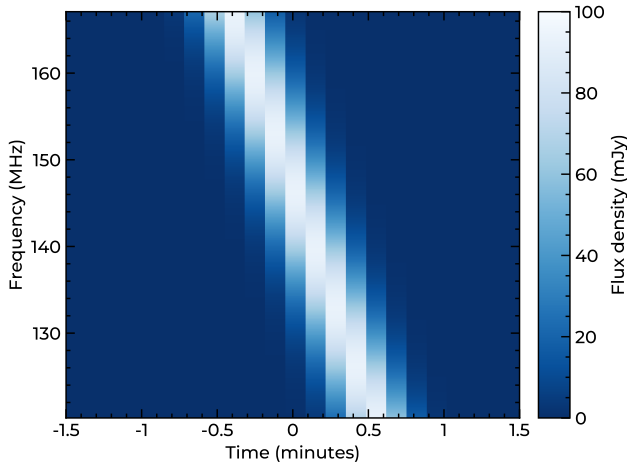
Declarations

- Conflict of interest: The authors do not have any conflicts of interest to report.
- Authors’ contributions: JRC initiated the LOFAR project that led to the discovery of the source, conducted the cross-matching analysis and wrote the paper. CT wrote the dynamic spectra software and helped interpret the data. RK identified the burst. HKV, JRC, RDK and PZarka led the

theoretical interpretation of the detection and contributed substantially to the paper. SBellotti and PIC obtained the Zeeman Doppler imaging data on the star. MJH and TWS processed the survey data. PZucca and HR provided solar physics expertise for interpreting the burst. SBloot, DCK, LL, EKP and BJSP commented on the paper and provided relevant expertise in characterizing StKM 1-1262. HJAR is the principal investigator of LoTSS and commented on the paper.

- **Data Availability:** LOFAR visibilities taken are publicly available via the LOFAR Long Term Archive (ObsID: 470106; LoTSS field: P236+53). The *XMM-Newton* data are available through the *XMM-Newton* Science Archive (XSA) (ObsID: 0401270201). All other data used in the manuscript have been sourced from the public domain.
- **Code Availability:** The important codes used to analyse and process the LOFAR data are available at the following sites: WSClean (<https://gitlab.com/aroffringa/wsclean>), DynSpecMS (<https://github.com/cyriltasse/DynSpecMS>), and DDF pipeline (<https://github.com/mhardcastle/ddf-pipeline>). The posteriors obtained from fitting a geometric flare model to the dynamic radio spectrum are available here: <https://github.com/robkavanagh/papers/tree/main/type-II>.
- **Correspondence:** Correspondence and requests for materials should be addressed to JRC and CT (email: callingham@astron.nl and cyril.tasse@obspm.fr).
- **Inclusion & Ethics statement:** All relevant ethics and inclusion principles for an astronomy project using data from LOFAR have been followed.

Extended Data



Extended Data Figure 1 Reconstruction of the burst assuming ECMI from a high-latitude coronal loop. While the overall drift rate is recovered, it is not possible to recover the observed sub-structure in Figure 1.

Extended Table 1 Fit parameters for the ECMI emission model. The uniform prior ranges and posteriors obtained for each parameter in our flaring loop model. The Julian Date for t_0 is 2457526.328. Note that the uncertainty on $\Delta\alpha$ is smaller than the lowest significant digit. The uncertainties presented in this table represent $1\text{-}\sigma$.

Parameter	Symbol	Prior	Posterior
Loop co-latitude ($^\circ$)	θ_l	[0, 90]	$16.65^{+1.36}_{-0.47}$
Loop longitude at time t_0 ($^\circ$)	ϕ_l	[-90, 90]	$-73.30^{+2.19}_{-4.15}$
Angle between loop and the meridian ($^\circ$)	δ_l	[0, 180]	$120.08^{+1.45}_{-3.30}$
Magnetic field strength at footpoint (G)	B_{fp}	[60, 10000]	$174.29^{+45.53}_{-40.88}$
Magnetic field gradient (G R_\star^{-1})	m	[0, 20000]	$9583.77^{+491.12}_{-754.81}$
Loop radius (R_\star)	L	[0, 0.5]	0.30 ± 0.02
Cone opening angle ($^\circ$)	α	[40, 90]	$77.42^{+0.88}_{-1.83}$
Cone thickness ($^\circ$)	$\Delta\alpha$	[0, 1]	0.01
Maximum flux density visible (mJy)	F_0	[0, 500]	$92.84^{+1.85}_{-1.90}$